Spectrally Resolved Hong-Ou-Mandel Interferometry with Discrete Color Entanglement

Congzhen Chen, Yuanyuan Chen,* and Lixiang Chen†
Department of Physics, Xiamen University, Xiamen 361005, China

(Received 26 October 2022; revised 15 February 2023; accepted 1 May 2023; published 30 May 2023)

Hong-Ou-Mandel (HOM) interferometry is a powerful quantum metrology technique to reconstruct the surface-depth profile of transparent samples with complementary benefits of measurement precision and experimental robustness. It is generally assumed that a trade-off exists between the standard HOM interferometry sensitivity and its ambiguity-free dynamic range. Here we challenge this "well-known" assumption through the implementation of spectrally resolved HOM interferometry with discrete color entanglement, and show that the well-separated frequencies embedded in a quantum state suffices to achieve great advantages in enhancing the temporal resolution but without limiting its ambiguity-free dynamic range. Backed by the Fisher-information analysis, spectrally resolved coincidence detection is an optimal measurement strategy as it enables us to recover the quantum Cramér-Rao bound. These results may significantly facilitate the use of spectrally resolved quantum interference for real-time quantum information processing, such as ultrafast phase transition and spectral-temporal photography.

DOI: 10.1103/PhysRevApplied.19.054092

I. INTRODUCTION

Quantum interference provides an alternative route towards enhancing the metrology and sensing technologies that are beyond the possibilities of classical physics [1–3]. Hong-Ou-Mandel (HOM) interference, the fact that two indistinguishable photons that arrive simultaneously at a balanced beam splitter would bunch into the identical output port, is a prototypical example of such a quantum phenomenon [4,5]. HOM interferometry can reconstruct the surface-depth profile of transparent samples without any requirement of temporal or spatial scanning [6–9], which provides complementary benefits and additional opportunities with respect to the classical metrology techniques. For example, HOM interferometry typically uses low-intensity light at single-photon level, which is crucial for delicate photoactive samples [9,10]. Since HOM interference is measured via photon correlation, the inherent stability and the robustness against perturbation are readily achieved as a direct result of biphoton quantum interference [11]. Thus, quantum metrology techniques based on HOM interference enable a wide range of quantum information processing tasks, ranging from the ultrasensitive metrology, high-resolution imaging, as well as high-dimensional quantum communication and computation [6,12–14].

In the context of such applications, indistinguishable photons are necessary prerequisites such that degenerate photons (identical spectral distribution) are typically used. Based on the theoretical prediction and experimental certification, it is generally known that the single-photon frequency bandwidth imposes the ultimate limit on the precision. The ultimate limit of a HOM-based sensor for estimating an unknown parameter τ of a physical system is known as the Cramér-Rao bound $\delta\tau$, which is attached to a particular probe state but is independent of any ingenious measurement procedure. Typically, indistinguishable photon pairs that are commonly used in the standard HOM interferometry allow us to achieve a bound as $\delta\tau = 1/(2\sigma\sqrt{N})$, where σ is the rms bandwidth of single photons, N represents the number of independent experimental trials [15]. Recently, two well-separated and entangled-discrete frequency modes and coincidence detection on a biphoton beat note are proposed that suffices to achieve great precision. Its sensitivity limits is mainly determined not only by the single-photon frequency bandwidth, but also by the difference frequencies of color-entangled photons. Thus, the use of two well-separated frequencies embedded in a quantum entangled state suffices to achieve a greater precision as $\delta\tau = 1/\sqrt{N(4\sigma^2 + \Delta^2)}$. Additionally, coincidence detection at two output ports of the HOM interferometry is certified as the optimal measurement strategy since it enables the recovery of the quantum Cramér-Rao bound [16]. However, this method faces the significant challenge of limited dynamic range. While the typical ambiguity-free measurement length of

*chenyy@xmu.edu.cn
†chenlx@xmu.edu.cn

the standard HOM interferometric sensor is fundamentally determined by the coherence time of single photons [17], the ambiguity-free dynamic range of HOM interferometry on a biphoton beat note is much shorter than the coherence time because of the periodic oscillation in the temporal detection [16,18,19]. As a direct consequence, the broad consensus has been that a trade-off exists between a HOM interferometry sensitivity and its ambiguity-free dynamic range [15,20]. On the other hand, the temporally resolved HOM interferometry has a notorious requirement for the precise scanning process in the temporal domain, and thus poses a serious obstacle for its use in real-time or ultrafast sensing applications.

To tackle this issue, spectrally resolved HOM interferometry is an alternative commonly used method in practical applications, which also promises enhancements in precision and sensitivity within a wide dynamic range [18, 21–23]. Since the spectrally resolved quantum interference pattern maps monotonically with respect to the unknown parameter τ, the corresponding ambiguity-free dynamic range is independent on temporal detection. Additionally, competing with the conventional temporal measurements, spectral detection in quantum interference provides an improvement in shorting the capturing time as two-photon joint-spectral intensity can be obtained from single measurement [18,24]. This scan-free technology enables a variety of real-time sensing applications such as ultrafast phase transition and spectral-temporal photography [25,26].

Here, we show that spectrally resolved HOM interferometry with discrete color entanglement is an optimal measurement strategy, wherein the ultimate bound $\delta\tau = 1/\sqrt{N(4\sigma^2+\Delta^2)}$ can be recovered and the ambiguity-free dynamic range is significantly widened. Building on the specific measurement-estimation strategy, the Fisher information is analyzed to determine the optimum sensing points in a practical experiment, and thus it enables the adaptive modulation to achieve the optimal measurement precision and accuracy even in the presence of imperfect experimental conditions. These results show that our approach provides a simple way of beating the temporal resolution limit but without limiting its ambiguity-free dynamic range, and may also indicate an alternative direction towards fully harnessing a biphoton spectral-temporal wave function in quantum metrology and quantum information processing [19,27–29].

II. CRAMÉR-RAO BOUND OF SPECTRALLY RESOLVED HOM INTERFEROMETRY

Let us consider an experimental configuration of spectrally resolved HOM interferometry as shown in Fig. 1 [15,16]. In the context of spectrally resolved HOM interferometry, the probe state is frequency entangled photon pairs that can be expressed as

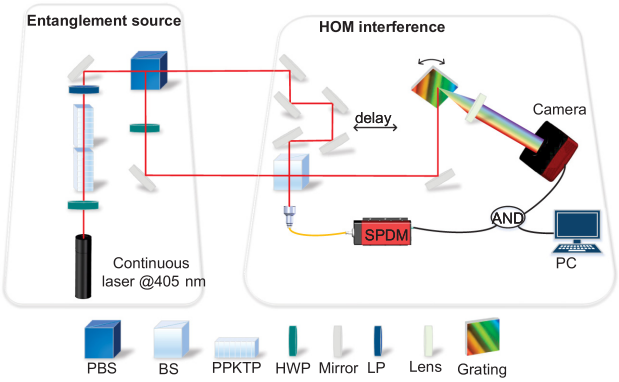

FIG. 1. Experimental setup of spectrally resolved HOM interferometry. HWP, half-wave plate; PPKTP, periodically poled potassium titanyl phosphate nonlinear crystal; LP, long-pass filter; PBS, polarizing beam splitter; BS, beam splitter; SPDM, single-photon detection module; AND, coincidence counts; grating, near-IR diffraction grating.

$$|\Psi(\tau)\rangle = \frac{1}{\sqrt{2}}\int d\Omega f(\Omega) \times \Big[e^{i(\Delta+2\Omega)\tau}a_1^\dagger(\Omega_s+\Omega)a_2^\dagger(\Omega_i-\Omega) - a_1^\dagger(\Omega_i+\Omega)a_2^\dagger(\Omega_s-\Omega)\Big]|\text{vac}\rangle, \quad (1)$$

where Ω_s and Ω_i are well-separated center frequencies embedded in a quantum entangled state, $\Delta = \Omega_s - \Omega_i$ is the difference frequency of these color-entangled photons, $|\text{vac}\rangle$ is the vacuum state, and $f(\Omega)$ is the Gaussian spectral amplitude function that fulfills the normalization condition as $\int d\Omega |f(\Omega)|^2 = 1$. As proved in Ref. [16], this particular probe state enables us to achieve the quantum Cramér-Rao bound as $\delta\tau = 1/\sqrt{N(4\sigma^2+\Delta^2)}$. Next we show that spectrally resolved HOM interference measurement is indeed an optimal strategy to recover this ultimate bound.

These paired photons are routed into the two input ports of a HOM interferometer, which transforms the incident state into

$$|\Psi(\tau)\rangle \to |\Phi_A(\tau)\rangle + |\Phi_B(\tau)\rangle, \quad (2)$$

where $|\Phi_A(\tau)\rangle$ and $|\Phi_B(\tau)\rangle$ correspond to the events that two photons emerge in opposite and identical outports, respectively. The normalized coincidence detection probability identified by single-photon detectors at distinct spatial modes reads

$$P_c(\tau,\omega)=\frac{1}{4\sqrt{2\pi\sigma^2}}[1-\cos((2\omega-\omega_p)\tau)]\left[\exp\left(-\frac{(\omega-\Omega_s)^2}{2\sigma^2}\right)+\exp\left(-\frac{(\omega-\Omega_i)^2}{2\sigma^2}\right)\right], \tag{3}$$

where ω is the frequency of one of the indistinguishable paired photons [24,30] (see Appendix for more details). In the case of a real HOM interferometer, that is subject to photon loss γ and imperfect experimental visibility α, there are three possible measurement outcomes; either both photons are detected as coincidence event, one photon is detected, or no photon is detected. The corresponding probability distributions read

$$\begin{aligned}
P_2(\tau,\omega)&=\frac{(1-\gamma)^2}{4\sqrt{2\pi\sigma^2}}[1+\cos((2\omega-\omega_p)\tau)]\left[\exp\left(-\frac{(\omega-\Omega_s)^2}{2\sigma^2}\right)+\exp\left(-\frac{(\omega-\Omega_i)^2}{2\sigma^2}\right)\right],\\
P_1(\tau,\omega)&=\frac{(1-\gamma)^2}{4\sqrt{2\pi\sigma^2}}\left[\frac{1+3\gamma}{1-\gamma}-\cos((2\omega-\omega_p)\tau)\right]\left[\exp\left(-\frac{(\omega-\Omega_s)^2}{2\sigma^2}\right)+\exp\left(-\frac{(\omega-\Omega_i)^2}{2\sigma^2}\right)\right],\\
P_0(\tau,\omega)&=\frac{\gamma^2}{2\sqrt{2\pi\sigma^2}}\left[\exp\left(-\frac{(\omega-\Omega_s)^2}{2\sigma^2}+\exp\left(-\frac{(\omega-\Omega_i)^2}{2\sigma^2}\right.\right.\right],
\end{aligned} \tag{4}$$

where subscripts 0, 1, and 2 denote the number of detectors that click, corresponding to total loss, bunching, and antibunching, respectively. For degenerate frequency-entangled photons ($\Delta=0$), the theoretical prediction and experimental observation of HOM interference patterns are shown in Fig. 2(a)–2(d). For nondegenerate frequency-entangled photons ($\Delta=5$ THz), the theoretical prediction and experimental observation of HOM interference patterns are shown in Fig. 3(a)–3(d). The outcome probabilities in this measurement can now be used to construct an estimator for the value of τ.

An estimator $\tilde{\tau}$ is a function of the experimental data that allows us to infer the value of the unknown time delay using a particular statistical model for the probability distribution of measurement outcomes. It is thus itself a random variable, that can be constructed from the probability distributions as a function of time delay. The average of an *unbiased estimator* corresponds to the real-time delay. For any such estimator, classical estimation theory states standard deviation is lower bounded by

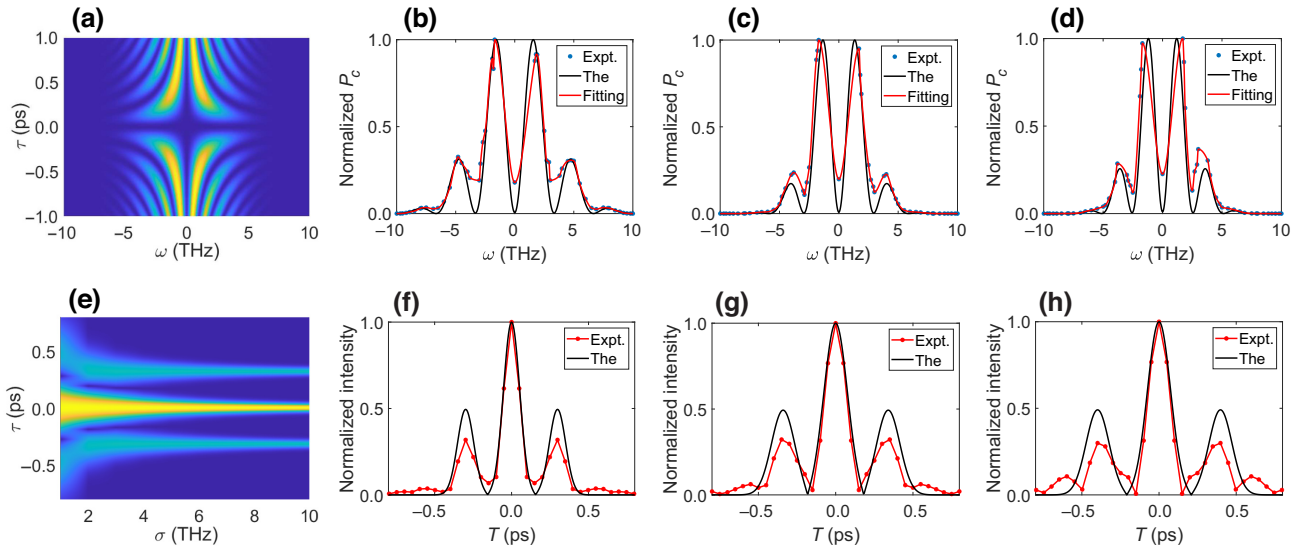

FIG. 2. Spectrally resolved HOM interferometry based on degenerate photons ($\Delta=0$). (a) Normalized interference probability as functions of the single-photon frequency and the relative time delay. (b) The normalized joint spectral intensity for time delays $\tau=0.30$ ps, (c) the normalized joint spectral intensity for time delays $\tau=0.34$ ps, and (c) the normalized joint spectral intensity for time delays $\tau=0.39$ ps. The single-photon frequency bandwidth σ is set as 4.24 THz. By performing a Fourier transform on the joint spectral intensities, the two-photon temporal signals are obtained as shown in (f)–(h). (e) The normalized temporal signals are calculated as functions of single-photon frequency bandwidth.

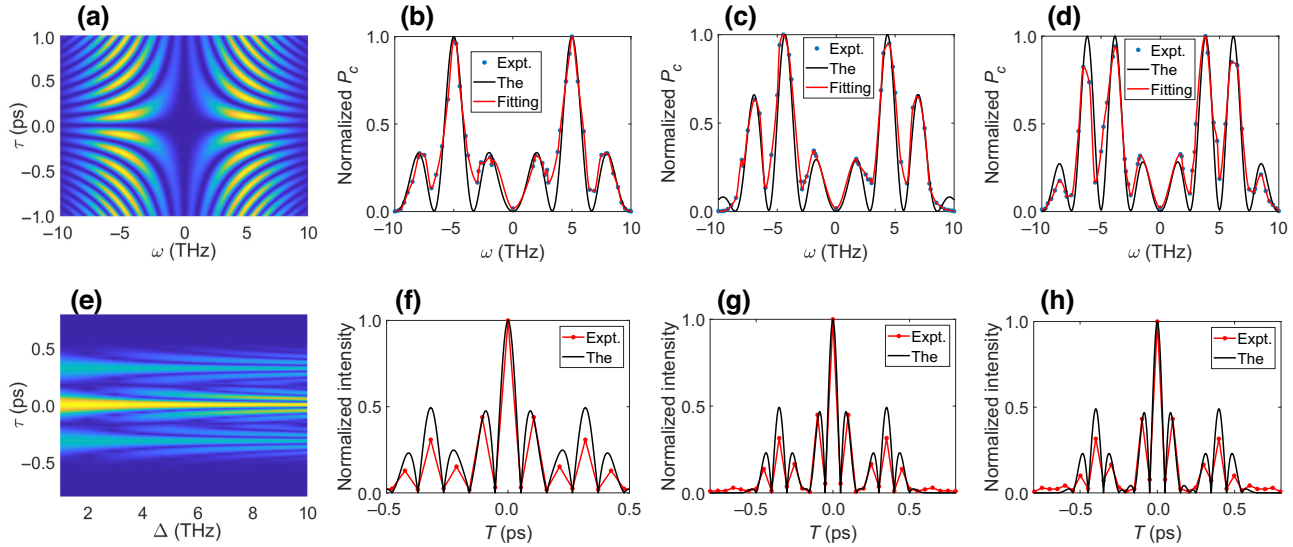

FIG. 3. Spectrally resolved HOM interferometry based on nondegenerate photons ($\Delta \neq 0$). (a) Normalized interference probability as functions of the single-photon frequency and the relative time delay. (b) The normalized joint spectral intensity for time delays $\tau = 0.30$ ps, (c) the normalized joint spectral intensity for time delays $\tau = 0.34$ ps, and (c) the normalized joint spectral intensity for time delays $\tau = 0.39$ ps. The single-photon frequency bandwidth σ is set as 4.24 THz, and the difference frequency Δ is set as 5 THz. By performing a Fourier transform on the joint spectral intensities, the two-photon temporal signals are obtained as shown in (f)–(h). (e) The normalized temporal signals are calculated as functions of single-photon frequency bandwidth.

$$\delta\tau_{\mathrm{CR}} = \frac{1}{(NF_\tau)^{1/2}} \geq \delta\tau_{\mathrm{QCR}}, \tag{5}$$

where the Fisher information F_τ reads

$$F_\tau = \int_{-\infty}^{\infty} d\omega \frac{(\partial_\tau P_2(\tau,\omega))^2}{P_2(\tau,\omega)} + \frac{(\partial_\tau P_1(\tau,\omega))^2}{P_1(\tau,\omega)} + \frac{(\partial_\tau P_0(\tau,\omega)^2}{P_0(\tau,\omega)}. \tag{6}$$

This value is tied to a particular quantum state and a specific measurement strategy. In a specific experiment (measurement strategy), the Fisher information quantifies the information that a particular measurement can reveal about the unknown parameter of interest. Note that optimizing over all probability distributions results we can recover the quantum Cramér-Rao bound, which states that this measurement strategy is optimal. Evaluating the Fisher information for this set of probabilities, we find that

$$F_\tau = \int_{-\infty}^{\infty} d\omega \frac{1}{\sqrt{2\pi\sigma^2}} \frac{(1-\gamma)^2(\gamma+1)(2\omega-\omega_p)^2}{[1+\alpha\cos((2\omega-\omega_p)\tau)]} \frac{\alpha^2\sin^2((2\omega-\omega_p)\tau)\left[\exp\left(-\frac{(\omega-\Omega_s)^2}{2\sigma^2}\right)+\exp\left(-\frac{(\omega-\Omega_i)^2}{2\sigma^2}\right)\right]}{2(1-\gamma)^2\left[\frac{1+3\gamma}{1-\gamma}-\alpha\cos((2\omega-\omega_p)\tau)\right]},$$

which is undefined at the position of $\tau = 0$ in the ideal experimental environment. We find that its upper bound is achieved in ideal case ($\gamma = 0, \alpha = 1$) as

$$\begin{aligned} F_\tau &\leq \int_{-\infty}^{\infty} d\omega \frac{\exp\left(-\frac{(\omega-\Omega_s)^2}{2\sigma^2}\right)+\exp\left(-\frac{(\omega-\Omega_i)^2}{2\sigma^2}\right)}{2\sqrt{2\pi\sigma^2}} \\ &\quad \times \frac{\sin^2((2\omega-\omega_p)\tau)(2\omega-\omega_p)^2}{1-\cos^2((2\omega-\omega_p)\tau)} \\ &= \Delta^2 + 4\sigma^2. \end{aligned} \tag{7}$$

In the case of zero loss and perfect visibility we recover the quantum Cramér-Rao bound, thus confirming that the measurement strategy is indeed optimal. In our experiment, the ultimate Fisher information that can be achieved is shown in Fig. 4, where Fig. 4(a) agrees well with the conventional HOM interferometry, and Fig. 4(b) agrees well with the HOM interferometry on a biphoton beat note. Additionally, these statistical prediction states that the optimal sensing position depends on the specific experimental parameters in the presence of imperfect visibility or photon loss.

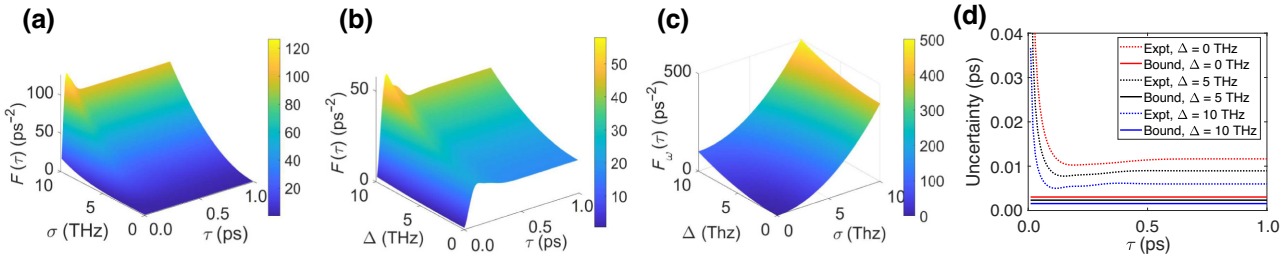

FIG. 4. Fisher information as functions of the relative time delay τ and (a) single-photon bandwidth σ with specific difference frequency $\Delta = 0$, (b) difference frequency Δ with specific single-photon bandwidth $\sigma = 4.24$ THz in the case of imperfect interference visibility $\alpha = 0.9$ and photon loss rate $\gamma = 0.2$. (c) The ultimate limit of Fisher information that can be achieved in our spectrally resolved HOM interferometry in the ideal case. (d) Measurement precision as a function of the relative time delay for various discrete color entanglement.

III. STATISTICAL ESTIMATION IN SPECTRALLY RESOLVED HOM INTERFEROMETRY

While the ultimate resolution limit of spectrally resolved HOM interferometry is provided in Eq. (7), we further show how to construct a suitable estimator for τ based on the observation of biphoton joint spectral distribution. Let us consider a conventional statistical analysis method based on the connection between a biphoton spectral and temporal wave function, which can directly reveal the enhanced resolution by using discrete frequency entanglement. Recent works propose a quantum Wiener-Khinchin theorem to state that two-photon joint spectral intensity and the cross-correlation of two-photon temporal signal can be connected by making a Fourier transform, which has various applications in quantum interferometric spectroscopy and quantum optical coherence tomography [24, 31]. In analogy to this approach, by performing a Fourier transform on the biphoton joint spectral distribution as demonstrated in Eq. (4), the correlation of two-photon temporal signals are obtained as

$$\begin{aligned} R(T) = \mathcal{F}^{-1}[P_2(\omega)] &= \int_{-\infty}^{\infty} P_2(\omega) e^{-i\omega T} d\omega \\ &\propto \cos(\Delta T)\exp(-\sigma^2 T^2) \\ &\quad + \cos[\Delta(T+\tau)]\exp[-\sigma^2(T+\tau)^2]/2 \\ &\quad + \cos[\Delta(T-\tau)]\exp[-\sigma^2(T-\tau)^2]/2, \end{aligned} \tag{8}$$

which obviously manifests itself as a main peak that is accompanied by two bilateral symmetrical side peaks. Thus, the optimal estimator $\tilde{\tau}$ is predicted as the temporal distance between the main and side peaks, which consequently fulfills the task of quantum metrology. As with the quantum interferometric metrology by using color-entangled photons as demonstrated in Ref. [16], the periodic oscillation appears within the two-photon temporal signals such that its pattern is more sensitive to relative time delay. For degenerate frequency-entangled photons ($\Delta = 0$, $\sigma = 4.24$ THz) that are used to detect the relative time delays at 0.39 ps, the correlation of two-photon temporal signals as a function of single-photon bandwidth is shown in Fig. 2(e). For simplicity, we show the absolute value of $R(T)$ such that the phase shifts in temporal domain are neglected. This indicates that the temporal bandwidth gets narrower as single-photon bandwidth increases, which agrees well with the well-known statement that the temporal resolution is dependent on the single-photon bandwidth. For nondegenerate frequency-entangled photons ($\Delta = 5$ THz, $\sigma = 4.24$ THz), the correlation of two-photon temporal signals as a function of difference frequencies of color-entangled photons is shown in Fig. 3(e). In addition to the envelope that is limited by single-photon bandwidth, the oscillation gets faster as difference frequency increases, which indicates that the temporal resolution can be extremely enhanced.

To this end, another widely used analytical technique is maximum-likelihood estimation (MLE). The likelihood function $\mathcal{L}(\tau)$ is defined from measurement outcomes, whose logarithm can be maximized by using optimization algorithm such as gradient descent to predict the parameter τ that we want to infer. In our framework, the likelihood function is a multinomial distribution as

$$\mathcal{L}(N_0^\omega, N_1^\omega, N_2^\omega|\tau) \propto \prod_\omega P_0(\tau,\omega)^{N_0^\omega} P_1(\tau,\omega)^{N_1^\omega} P_2(\tau,\omega)^{N_2^\omega}, \tag{9}$$

where N_0^ω, N_1^ω, and N_2^ω denote the numbers of events that no, only one and two detector(s) click(s) for single photons at a center frequency of ω, respectively. Note that $P_0(\tau,\omega)$, being independent of τ, results in a constant scale factor that is of no relevance to the final calculation of the Fisher information and parameter estimation. The likelihood is

extremized as [15]

$$0 =: (\partial_\tau log\mathcal{L})_{\tilde{\tau}_{\mathrm{MLE}}} = \sum_\omega \frac{N_0^\omega P_0(\tau,\omega)'}{P_0(\tau,\omega)} + \frac{N_1^\omega P_1(\tau,\omega)'}{P_1(\tau,\omega)} + \frac{N_2^\omega P_2(\tau,\omega)'}{P_2(\tau,\omega)}, \tag{10}$$

and solving this equation enables us to predict an optimal estimator as $\tilde{\tau}_{\mathrm{MLE}}$. Here $P_1(\tau,\omega)$ is independent on the parameter of interest τ, and thus it can be neglected. Based on the calculation in Eq. (3), we know that $P_1(\tau,\omega)' = P_2(\tau,\omega)'$ such that the likelihood function is simplified as

$$0 = \sum_\omega \frac{N_1^\omega}{P_1(\tau,\omega)} + \frac{N_2^\omega}{P_2(\tau,\omega)}. \tag{11}$$

We note that the values of parameters α, γ, σ, and Δ needs to be separately estimated before the measurement begin.

IV. EXPERIMENTAL IMPLEMENTATION OF SPECTRALLY RESOLVED HOM INTERFEROMETRY

As shown in Fig. 1, paired signal and idler photons are prepared by spontaneous parametric down-conversion (SPDC) in the nonlinear crystals that is pumped with a continuous-wave pump laser. As the difference frequencies of down-converted signal and idler photons typical exceed the spectral bandwidth of the pump photons, frequency entanglement arises quite naturally as a direct result of energy conservation. In order to tune the difference frequency flexibly, two nonlinear crystals with type-II SPDC are placed in sequence, wherein the optical axis of the second crystal is rotated by 90° with respect to the first. Therefore, the balanced pumping of two crystal results in equal probability amplitudes for SPDC emission $|H,\omega_p\rangle \rightarrow |H,\omega_s\rangle|V,\omega_i\rangle$ in the first crystal, or $|V,\omega_p\rangle \rightarrow |V,\omega_s\rangle|H,\omega_i\rangle$ in the second crystal, where H and V denote horizontal and vertical polarizations, and $\omega_{p/s/i}$ represent the center frequencies of pump, signal and idler photons [32,33]. This created frequency-entangled state can be written as

$$|\psi\rangle \rightarrow \frac{1}{\sqrt{2}}(|\omega_s\rangle|\omega_i\rangle - |\omega_i\rangle|\omega_s\rangle) \otimes |H\rangle|V\rangle. \tag{12}$$

A polarizing beam splitter is used to map the orthogonally polarized photon pairs into the input ports of a beam splitter. The detection probability can be observed by scanning the arriving time of one of the paired photons incident on the beam splitter, which constitutes a HOM interferometer. One output port of the coupler is directly connected to a single-photon counting module (SPCM), while a Bragg grating is inserted between the other output port and SPCM to map the continuous spectrum into the spatial distribution. In our experimental implementation, the grating provides a spectral resolution with respect to spatial separation as 0.4 nm/10 μm. The coincidences are identified between the distinct output ports of the beam splitter when two photons arrive at the detectors within a temporal window of approximately 1 ns. Figures 2(a)–2(d) and 3(a–d) show the theoretical and experimental measurement results of the normalized coincidence probabilities with respect to the relative time delay and the difference frequencies.

For degenerate frequency-entangled photon pairs ($\Delta = 0$), the joint spectral distributions for time delays $\tau = 0.30$, 0.34, and 0.39 ps are shown in Fig. 2(b)–2(d), wherein the single-photon frequency bandwidth is approximately 4.24 THz, corresponds to a coherence time of 0.24 ps. By performing a Fourier transform on the joint spectral function, the correlation of two-photon temporal signal are obtained as shown in Fig. 2(f)–2(h), which enables us to extract the estimator of τ. According to the analysis of Fisher information in Eq. (7), the ultimate Cramér-Rao bound of measurement precision depends on the single-photon frequency bandwidth σ. More specifically, the temporal bandwidth achieved in the correlation of two-photon temporal signal becomes narrower with respect to the increase of σ as shown in Fig. 2(a), namely it is easier to obtain the temporal distance between peaks in the correlation patterns. This agrees well with the theoretical prediction that the Fisher information can be increased by using photons with broader spectral distribution as shown in Fig. 4(a).

By using nondegenerate frequency-entangled photon pairs ($\Delta \neq 0$), the joint spectral distributions for time delay $\tau = 0.30$ ps, 0.34 ps, and 0.39 ps are shown in Fig. 3(b)–3(d). Analogously, by performing a Fourier transform on the joint spectral function, the correlation of two-photon temporal signal are obtained as shown in Fig. 3(f)–3(h). It is interesting to find that the oscillation appears in the typical Gaussian envelopes, which is determined by the difference frequency Δ. As shown in Fig. 3(d), the periodic oscillation in the correlation patterns makes it easier to obtain the temporal distance, which indicates the estimator of τ. As verified by the analysis of Fisher information in Eq. (7), the ultimate Cramér-Rao bound of measurement precision can be further enhanced by Δ. This agrees well with our previous work that the Fisher information can be increased by using discrete color-entangled photons with larger difference frequency as shown in Fig. 4(b). As a direct result, the Fisher information of spectrally resolved HOM interferometry is determined by both of single-photon spectral distribution and difference frequency of discrete color entanglement as shown in Fig. 4(c). The resultant measurement precision for various relative time delay is shown in Fig. 4(d).

In the standard HOM interferometry by using degenerate photons with single-photon frequency bandwidth of

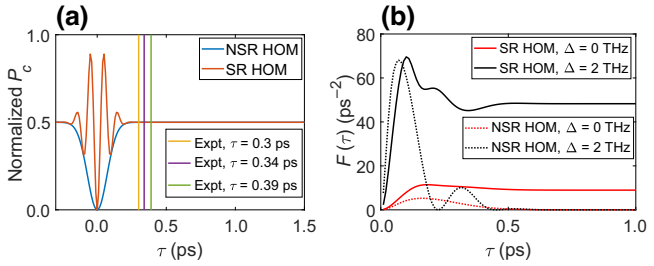

FIG. 5. Comparison of the ambiguity-free dynamic ranges between the temporally resolved HOM interferometry (NSR HOM) and spectrally resolved HOM interferometry (SR HOM). (a) The HOM interference pattern for degenerate photons and color entanglement with $\sigma = 4.24$ THz and $\Delta = 5$ THz. The three vertical lines represent the time delays that are estimated in our experiment, which are utterly beyond the coherence time of HOM interference envelope. (b) The theoretically calculated Fisher information for the temporally and spectrally resolved HOM interferometry in the nonideal case of $\alpha = 0.9$ and $\gamma = 0.2$. In order to clearly show their comparison, we reset $\sigma = 1.5$ THz and $\Delta = 2$ THz.

approximately 4.24 THz, its ambiguity-free measurement length is fundamentally determined by the corresponding coherence time of 0.24 ps [17]. However, as illustrated in Fig. 5(a), the relative time delays to be tested in our proof-of-principle experiments are $\tau = 0.30$ ps, 0.34 ps, and 0.39 ps, which are obviously longer than the coherence time. Namely, our technique enables the observation of the HOM interference patterns for a longer time delay than that in the standard HOM interference. For an instructive means of understanding, we demonstrate the achievable Fisher information in Fig. 5(b). Thereinto, it is obvious that the Fisher information of temporally resolved (nonspectrally resolved) HOM interferometry decays with respect to the relative time delay, namely its dynamic range is limited by the coherence time of single photons. In contrast, the Fisher information of spectrally resolved HOM interferometry increases versus the time delay within the coherence time, and almost remains stable beyond the coherence time that still enables the precise estimation. As a direct result, these theoretical analysis and experimental results prove that the spectrally resolved HOM interferometry has the potential to extend the ambiguity-free dynamic range of the phase-shift measurement and timing synchronization [18]. In the meanwhile, we note that the dynamic range of this spectrally resolved HOM interferometry would be limited by the resolution of single-photon spectrometer.

V. DISCUSSION

We present a viable scheme to implement spectrally resolved HOM interferometry for achieving great precision and sensitivity in measuring optical delays within a wide dynamic range. Additionally, we also show that the exploitation of discrete frequency-entangled photons enables the conventional temporal resolution limit to be beaten, and the spectrally resolved coincidence detection is an optimal measurement strategy since it enables us to recover the quantum Cramér-Rao bound. This spectrally resolved HOM interferometry provides complementary benefits such as low-light imaging for photonsensitive biological and chemical molecules [9], robustness against perturbation and noise [34], cancellation of some deleterious dispersion effects [11,35,36], and shorting the capturing time for real-time and ultrafast photography. Due to these results and benefits, our approach has the potential to be an ideal candidate for more quantum enhanced metrology applications [19,27–29].

Although this work reports only the advantages of our approach in estimation of the depth profile, similar great enhancement can also be achieved for a variety of applications like state discrimination or hypothesis testing.

ACKNOWLEDGMENTS

This work is supported by the National Natural Science Foundation of China (91636109, 11904303), the Fundamental Research Funds for the Central Universities at Xiamen University (20720190054, 20720190057), the Natural Science Foundation of Fujian Province of China for Distinguished Young Scientists (2015J06002), and the program for New Century Excellent Talents in University of China (NCET-13-0495).

APPENDIX: SPECTRALLY RESOLVED HOM INTERFERENCE WITH FREQUENCY-ENTANGLED STATES

To make the calculation clearer, we simplify the input frequency-entangled states as shown in Eq. (1) to the form of

$$|\psi\rangle = \int_0^\infty \int_0^\infty d\omega_s d\omega_i f(\omega_s, \omega_i) \hat{a}_s^\dagger(\omega_s) \hat{a}_i^\dagger(\omega_i) |0\rangle, \quad \text{(A1)}$$

where $f(\omega_s, \omega_i)$ is the spectral amplitude function of frequency entanglement that fulfills the normalized condition as $\int\int d\omega_s d\omega_i |f(\omega_s, \omega_i)|^2 = 1$. In the ideal case, the HOM interference measurement is accomplished by using a lossless and balanced beam splitter. The beam-splitter transformation on the input modes can be expressed by

$$\hat{a}_s^\dagger(\omega_s) = \frac{1}{\sqrt{2}}[\hat{a}_1^\dagger(\omega_s) + \hat{a}_2^\dagger(\omega_s)],$$
$$\hat{a}_i^\dagger(\omega_s) = \frac{1}{\sqrt{2}}[\hat{a}_1^\dagger(\omega_i) - \hat{a}_2^\dagger(\omega_i)]. \quad \text{(A2)}$$

As a relative time delay τ is introduced by a transparent sample, it results in a phase shift $\exp(-i\omega_i\tau)$ that transmits

the two-photon state as $|\psi(\tau)\rangle \rightarrow |\psi_A(\tau)\rangle + |\psi_B(\tau)\rangle$

$$|\psi(\tau)\rangle = \frac{1}{2}\int_0^\infty\int_0^\infty d\omega_s d\omega_i f(\omega_s,\omega_i)e^{-i\omega_i\tau}[i\hat{a}_1^\dagger(\omega_s)\hat{a}_1^\dagger(\omega_i) + i\hat{a}_2^\dagger(\omega_s)\hat{a}_2^\dagger(\omega_i) + \hat{a}_1^\dagger(\omega_i)\hat{a}_2^\dagger(\omega_s) - \hat{a}_1^\dagger(\omega_s)\hat{a}_2^\dagger(\omega_i)]|0\rangle, \tag{A3}$$

where the subscripts 1/2 represent two output modes of the beam splitter, and

$$\begin{aligned}|\psi_A(\tau)\rangle &= \frac{1}{2}\int_0^\infty\int_0^\infty d\omega_s d\omega_i[f(\omega_s,\omega_i)e^{-i\omega_i\tau} - f(\omega_i,\omega_s)e^{-i\omega_s\tau}]\hat{a}_1^\dagger(\omega_s)\hat{a}_2^\dagger(\omega_i)|0\rangle,\\ |\psi_B(\tau)\rangle &= \frac{1}{2}\int_0^\infty\int_0^\infty d\omega_s d\omega_i[f(\omega_s,\omega_i)e^{-i\omega_i\tau} - f(\omega_i,\omega_s) e^{-i\omega_s\tau}](\hat{a}_1^\dagger(\omega_s)\hat{a}_1^\dagger(\omega_i) + \hat{a}_2^\dagger(\omega_s)\hat{a}_2^\dagger(\omega_i))|0\rangle.\end{aligned} \tag{A4}$$

Since the spectrally resolved HOM interference pattern is identified in opposite spatial modes resulting from anti-bunching effect, we focus on the calculation of $P_c(\tau) = |\langle\psi(\tau)|\psi_A(\tau)\rangle|^2$. It is obvious that two photons after the beam splitter are indistinguishable, we substitute ω_s and ω_i with ω_1 and ω_2. By multiplying $e^{-i\omega_i\tau}$ to cancel the global phase, we obtain

$$|\psi_A(\tau)\rangle = \frac{1}{2}\int_0^\infty\int_0^\infty d\omega_1 d\omega_2[f(\omega_1,\omega_2) - f(\omega_2,\omega_1) e^{-i(\omega_1-\omega_2)\tau}]\hat{a}_1^\dagger(\omega_1)\hat{a}_2^\dagger(\omega_2)|0\rangle. \tag{A5}$$

The detection operators of two detectors in different output modes are

$$\begin{aligned}\hat{E}_1^{(+)} &= \frac{1}{\sqrt{2\pi}}\int_0^\infty d\omega_1\hat{a}_1(\omega_1)e^{-i\omega_1 t_1},\\ \hat{E}_2^{(+)} &= \frac{1}{\sqrt{2\pi}}\int_0^\infty d\omega_2\hat{a}_2(\omega_2)e^{-i\omega_2 t_2}.\end{aligned} \tag{A6}$$

Thus the normalized coincidence probability $P(\tau)$ as a function of time delay can be expressed as

$$\begin{aligned}P_c(\tau) &= \langle\psi_A(\tau)|\hat{E}_1^{(-)}\hat{E}_2^{(-)}\hat{E}_2^{(+)}\hat{E}_1^{(+)}|\psi_A(\tau)\rangle\\ &= \frac{1}{4}\int_0^\infty\int_0^\infty d\omega_1 d\omega_2[|f(\omega_1,\omega_2)|^2 + |f(\omega_2,\omega_1)|^2 - 2f(\omega_1,\omega_2)f(\omega_2,\omega_1)\cos(\omega_1-\omega_2)\tau].\end{aligned} \tag{A7}$$

By substituting the function $f(\omega_1,\omega_2)$ with the joint spectral intensity of frequency entanglement, the simplified result is shown in Eq. (3).

[1] Roman Schnabel, Nergis Mavalvala, David E. McClelland, and Ping K. Lam, Quantum metrology for gravitational wave astronomy, Nat. Commun. **1**, 1 (2010).

[2] Zu-En Su, Yuan Li, Peter P. Rohde, He-Liang Huang, Xi-Lin Wang, Li Li, Nai-Le Liu, Jonathan P. Dowling, Chao-Yang Lu, and Jian-Wei Pan, Multiphoton Interference in Quantum Fourier Transform Circuits and Applications to Quantum Metrology, Phys. Rev. Lett. **119**, 080502 (2017).

[3] Vittorio Giovannetti, Seth Lloyd, and Lorenzo Maccone, Advances in quantum metrology, Nat. Photon. **5**, 222 (2011).

[4] C. K. Hong, Z. Y. Ou, and L. Mandel, Measurement of Subpicosecond Time Intervals Between Two Photons by Interference, Phys. Rev. Lett. **59**, 2044 (1987).

[5] Raphael Lopes, Almazbek Imanaliev, Alain Aspect, Marc Cheneau, Denis Boiron, and Christoph I. Westbrook, Atomic Hong-Ou-Mandel experiment, Nature **520**, 66 (2015).

[6] Bienvenu Ndagano, Hugo Defienne, Dominic Branford, Yash D. Shah, Ashley Lyons, Niclas Westerberg, Erik M. Gauger, and Daniele Faccio, Quantum microscopy based on Hong-Ou-Mandel interference, Nat. Photon. **16**, 384 (2022).

[7] Fabrice Devaux, Alexis Mosset, Paul-Antoine Moreau, and Eric Lantz, Imaging Spatiotemporal Hong-Ou-Mandel Interference of Biphoton States of Extremely High Schmidt Number, Phys. Rev. X **10**, 031031 (2020).

[8] V. Freulon, A. Marguerite, J.-M. Berroir, B. Plaçais, A. Cavanna, Y. Jin, and Gwendal Fève, Hong-Ou-Mandel experiment for temporal investigation of single-electron fractionalization, Nat. Commun. **6**, 1 (2015).

[9] Audrey Eshun, Bing Gu, Oleg Varnavski, Shahaf Asban, Konstantin E. Dorfman, Shaul Mukamel, and Theodore Goodson III, Investigations of molecular optical properties using quantum light and Hong-Ou-Mandel interferometry, J. Am. Chem. Soc. **143**, 9070 (2021).

[10] A. Thoma, P. Schnauber, M. Gschrey, M. Seifried, J. Wolters, J.-H. Schulze, A. Strittmatter, S. Rodt, A. Carmele, A. Knorr, T. Heindel, and S. Reitzenstein, Exploring Dephasing of a Solid-State Quantum Emitter via Time- and Temperature-Dependent Hong-Ou-Mandel Experiments, Phys. Rev. Lett. **116**, 033601 (2016).

[11] Magued B. Nasr, Bahaa E. A. Saleh, Alexander V. Sergienko, and Malvin C. Teich, Demonstration of Dispersion-Canceled Quantum-Optical Coherence Tomography, Phys. Rev. Lett. **91**, 083601 (2003).

[12] Toshiki Kobayashi, Rikizo Ikuta, Shuto Yasui, Shigehito Miki, Taro Yamashita, Hirotaka Terai, Takashi Yamamoto, Masato Koashi, and Nobuyuki Imoto, Frequency-domain Hong–Ou–Mandel interference, Nat. Photon. **10**, 441 (2016).

[13] Yuanyuan Chen, Qian Shen, Song Luo, Long Zhang, Zhanghai Chen, and Lixiang Chen, Entanglement-Assisted Absorption Spectroscopy by Hong-Ou-Mandel Interference, Phys. Rev. Appl. **17**, 014010 (2022).

[14] Daniele Cozzolino, Beatrice Da Lio, Davide Bacco, and Leif Katsuo Oxenløwe, High-dimensional quantum communication: Benefits, progress, and future challenges, Adv. Quantum Technol. **2**, 1900038 (2019).

[15] Ashley Lyons, George C. Knee, Eliot Bolduc, Thomas Roger, Jonathan Leach, Erik M. Gauger, and Daniele Faccio,

Attosecond-resolution Hong-Ou-Mandel interferometry, Sci. Adv. **4**, eaap9416 (2018).

[16] Yuanyuan Chen, Matthias Fink, Fabian Steinlechner, Juan P. Torres, and Rupert Ursin, Hong-Ou-Mandel interferometry on a biphoton beat note, npj Quantum Inf. **5**, 1 (2019).

[17] Dimitry Yankelev, Chen Avinadav, Nir Davidson, and Ofer Firstenberg, Atom interferometry with thousand-fold increase in dynamic range, Sci. Adv. **6**, eabd0650 (2020).

[18] Rui-Bo Jin, Ryosuke Shimizu, Mikio Fujiwara, Masahiro Takeoka, Ryota Wakabayashi, Taro Yamashita, Shigehito Miki, Hirotaka Terai, Thomas Gerrits, and Masahide Sasaki, Simple method of generating and distributing frequency-entangled qudits, Quantum Sci. Technol. **1**, 015004 (2016).

[19] Yaniv Eliezer, Liran Hareli, Lilya Lobachinsky, Sahar Froim, and Alon Bahabad, Breaking the Temporal Resolution Limit by Superoscillating Optical Beats, Phys. Rev. Lett. **119**, 043903 (2017).

[20] Chen Avinadav, Dimitry Yankelev, Ofer Firstenberg, and Nir Davidson, Composite-Fringe Atom Interferometry for High-Dynamic-Range Sensing, Phys. Rev. Appl. **13**, 054053 (2020).

[21] Malvin Carl Teich, Bahaa E. A. Saleh, Franco N. C. Wong, and Jeffrey H. Shapiro, Variations on the theme of quantum optical coherence tomography: A review, Quantum Inf. Process. **11**, 903 (2012).

[22] Pablo Yepiz-Graciano, Alí Michel Angulo Martínez, Dorilian Lopez-Mago, Hector Cruz-Ramirez, and Alfred B. U'Ren, Spectrally resolved Hong-Ou-Mandel interferometry for quantum-optical coherence tomography, Photon. Res. **8**, 1023 (2020).

[23] Zeferino Ibarra-Borja, Carlos Sevilla-Gutiérrez, Roberto Ramírez-Alarcón, Hector Cruz-Ramírez, and Alfred B. U'Ren, Experimental demonstration of full-field quantum optical coherence tomography, Photon. Res. **8**, 51 (2020).

[24] Yuanyuan Chen and Lixiang Chen, Quantum Wiener-Khinchin Theorem for Spectral-Domain Optical Coherence Tomography, Phys. Rev. Appl. **18**, 014077 (2022).

[25] Chengshuai Yang, Fengyan Cao, Dalong Qi, Yilin He, Pengpeng Ding, Jiali Yao, Tianqing Jia, Zhenrong Sun, and Shian Zhang, Hyperspectrally Compressed Ultrafast Photography, Phys. Rev. Lett. **124**, 023902 (2020).

[26] Yu Lu, Terence T. W. Wong, Feng Chen, and Lidai Wang, Compressed Ultrafast Spectral-Temporal Photography, Phys. Rev. Lett. **122**, 193904 (2019).

[27] Haowei Shi, Zheshen Zhang, Stefano Pirandola, and Quntao Zhuang, Entanglement-Assisted Absorption Spectroscopy, Phys. Rev. Lett. **125**, 180502 (2020).

[28] B. Brecht, Dileep V. Reddy, C. Silberhorn, and M. G. Raymer, Photon Temporal Modes: A Complete Framework for Quantum Information Science, Phys. Rev. X **5**, 041017 (2015).

[29] Yuanyuan Chen, Sebastian Ecker, Lixiang Chen, Fabian Steinlechner, Marcus Huber, and Rupert Ursin, Temporal distinguishability in Hong-Ou-Mandel interference for harnessing high-dimensional frequency entanglement, npj Quantum Inf. **7**, 1 (2021).

[30] S. Ramelow, L. Ratschbacher, A. Fedrizzi, N. K. Langford, and A. Zeilinger, Discrete Tunable Color Entanglement, Phys. Rev. Lett. **103**, 253601 (2009).

[31] Rui-Bo Jin and Ryosuke Shimizu, Extended Wiener-Khinchin theorem for quantum spectral analysis, Optica **5**, 93 (2018).

[32] Yuanyuan Chen, Sebastian Ecker, Sören Wengerowsky, Lukas Bulla, Siddarth Koduru Joshi, Fabian Steinlechner, and Rupert Ursin, Polarization Entanglement by Time-Reversed Hong-Ou-Mandel Interference, Phys. Rev. Lett. **121**, 200502 (2018).

[33] Yuanyuan Chen, Sebastian Ecker, Jessica Bavaresco, Thomas Scheidl, Lixiang Chen, Fabian Steinlechner, Marcus Huber, and Rupert Ursin, Verification of high-dimensional entanglement generated in quantum interference, Phys. Rev. A **101**, 032302 (2020).

[34] Hamish Scott, Dominic Branford, Niclas Westerberg, Jonathan Leach, and Erik M. Gauger, Noise limits on two-photon interferometric sensing, Phys. Rev. A **104**, 053704 (2021).

[35] Aephraim M. Steinberg, Paul G. Kwiat, and Raymond Y. Chiao, Dispersion cancellation and high-resolution time measurements in a fourth-order optical interferometer, Phys. Rev. A **45**, 6659 (1992).

[36] Ayman F. Abouraddy, Magued B. Nasr, Bahaa E. A. Saleh, Alexander V. Sergienko, and Malvin C. Teich, Quantum-optical coherence tomography with dispersion cancellation, Phys. Rev. A **65**, 053817 (2002).